Steady-State Diffusion

F. Liu, S. M. Abel, L. F. Collins,
B. R. Srijanto, R. Standaert, J. Katsaras,
C. P. Collier* 1900054

Geometry-Dependent Nonequilibrium Steady-State Diffusion and Adsorption of Lipid Vesicles in Micropillar Arrays

Adsorption from aqueous solution of monodisperse unilamellar lipid vesicles in the confined environments of ordered, hydrophilic micropillar arrays results in nonuniform fluorescence profiles on the pillars due to nonequilibrium steady-state formation of lipid density gradients on the pillars. These gradients result from the surface diffusion of adsorbed lipid membrane fragments on the pillar sidewalls and base substrate.

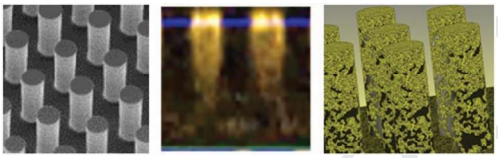

UNCORRECTED PROOF

ADVANCED MATERIALS INTERFACES
www.advmatinterfaces.de

Geometry-Dependent Nonequilibrium Steady-State Diffusion and Adsorption of Lipid Vesicles in Micropillar Arrays

*Fangjie Liu, Steven M. Abel, Liam F. Collins, Bernadeta R. Srijanto, Robert Standaert, John Katsaras, and C. Patrick Collier**

Micro- and nanofabricated sample environments are useful tools for characterizing diffusion in confined aqueous environments. The steady-state diffusion and adsorption of unilamellar lipid vesicles in arrays of hydrophilic micropillars is investigated. Gradients in the coverage of fluorescently labeled, pillar-supported lipid films, formed from vesicle fusion, are determined from 3D z-stack images using confocal microscopy. The gradients are the result of preferential adsorption of vesicles near the tops of the pillars, which progressively deplete them from solution as they diffuse toward the base of the array. However, the increased propensity for vesicle adsorption near the pillar tops compared to the confined spaces between pillars results in the formation of confluent supported lipid bilayers at the pillar tops that resist the adsorption of additional vesicles while leaving the pillar surfaces below available for binding. This results in a reduction in the numbers of depleted vesicles compared to what one would anticipate based on diffusive fluxes. The resulting inhomogeneous spatial profiles of lipid structures on the pillars are the result of the system being maintained in a dissipative, nonequilibrium steady state during incubation of the pillar arrays in the vesicle solution, which is ultimately quenched by rinsing away the unbound, freely diffusing vesicles.

1. Introduction

Transport of biological matter occurs in the confined and crowded aqueous environments of cells and subcellular compartments. As such, a better understanding of both active and passive transport at the micro- and nanoscale length scales is needed for advances in a number of biomedical applications such as drug delivery and adsorption,[1–8] tissue engineering, and regenerative medicine.[9,10] Embryonic growth and development mechanisms also depend on diffusion, as does tumor growth and metastasis. Adsorbed liposomes onto structured surfaces can form fluid, supported lipid bilayers as realistic models for biomembranes capable of mimicking cellular functions such as transport and signaling.[11–15] Micro- and nanopatterned surfaces can be utilized to mimic the geometries and scales of these environments, and to elucidate how biological phenomena that rely on diffusive transport are impacted in these spatially restricted environments.[16–18]

The geometrical and topological effects of micro- and nanofabricated structures on the diffusion and absorptive behavior of particles have been investigated both experimentally,[19–22] and with theoretical and numerical models.[23–29] Cylindrical pillar arrays have been commonly used to mimic the cytoskeleton and uncover its roles in modulating transport processes.[14,20,30,31] The hindered diffusion of particles due to cytoskeletal barriers has been modeled as diffusion in periodic arrays of obstacles.[24] More recent studies include investigations into the diffusive dynamics of nanoparticles confined in nanofabricated pillar arrays.[21,32,33] Adsorption rates of solute particles onto planar, spherical, and cylindrical surfaces have also been studied,[28] where it was discovered that surface geometry could be used to control the rates of adsorption.[28,30] These studies have focused on time-dependent diffusive dynamics at the single-particle or single-molecule level using single-particle tracking techniques or by monitoring the stochastic fluctuations of particles/molecules at equilibrium with fluctuation correlation analyses such as fluorescence correlation spectroscopy (FCS),[19] or by measuring the relaxation times of systems of particles/molecules at the bulk level with techniques such as fluorescence recovery after photobleaching (FRAP).[29]

In this paper, we investigated the *steady-state* diffusion and adsorption of nearly monodisperse liposomes (130 nm average diameter unilamellar lipid vesicles) in aqueous solution confined in micropillar arrays with a micropillar diameter of 5 µm, a center-to-center separation of 10 µm, and heights ranging

F. Liu, L. F. Collins, B. R. Srijanto, C. P. Collier
Center for Nanophase Materials Sciences
Oak Ridge National Laboratory
Oak Ridge, TN 37831, USA
E-mail: colliercp@ornl.gov
S. M. Abel
Department of Chemical and Biomolecular Engineering
University of Tennessee Knoxville
Knoxville, TN 37996, USA
R. Standaert
Department of Chemistry
Eastern Tennessee State University
Johnson City, TN 37614, USA
J. Katsaras
Neutron Sciences Directorate
Oak Ridge National Laboratory
Oak Ridge, TN 37831, USA
The ORCID identification number(s) for the author(s) of this article can be found under https://doi.org/10.1002/admi.201900054.

DOI: 10.1002/admi.201900054

UNCORRECTED PROOF

 © 2019 WILEY-VCH Verlag GmbH & Co. KGaA, Weinheim

from 1.5 to 17 µm. While steady-state measurements do not directly provide kinetic rates, they do provide spatiotemporal information found in stationary states characterized by gradients and other patterns that require the continuous production and removal of matter and energy. Here, the source of the steady state was the net diffusive flux of vesicles from the bulk solution, and the sink was the hydrophilic surfaces of the pillars and the base substrate of the pillar array. Effective steady-state diffusive fluxes of vesicles in solution to the pillar sidewalls and the base of the array were deduced a posteriori from 3D z-stack images captured on a laser scanning confocal fluorescence microscope. These resulted in intensity profiles of fluorescently labeled lipids in supported bilayers formed from the adsorption and fusion of liposomes to the hydrophilic silica surfaces. The fluorescent gradients on the pillar sidewalls extending from the pillar tops down toward the base of the pillar array could be fit with Gaussian functions. Fluorescent intensities at the base of the array between pillars ranged from being indistinguishable from those on the sidewalls for the shortest (1.5 µm) pillars, to being almost undetectable for the tallest (17 µm) pillars, the result of progressive depletion of vesicles from solution in the pillar arrays with increasing pillar height. These findings were consistent with kinetic Monte Carlo (kMC) simulations of particles representing liposomes in solution undergoing random walks in an array of pillars, and with finite element methods that numerically solved the diffusion equation at steady state with appropriate boundary conditions.

We attribute these findings to changes in steady-state diffusive flux as functions of pillar height and confinement in the micropillar array, coupled to surface processes involved in the formation of fluid supported lipid films on the pillars due to vesicle fusion. The experimentally measured fluorescent gradients were not as steep as predicted by the calculated molar diffusive fluxes obtained from kMC simulations and solutions of the diffusion equation, due to the formation of supported lipid bilayers at the tops of the pillars that blocked the adsorption of additional vesicles. This resulted in a net reduction in the numbers of vesicles depleted from solution compared to those predicted from diffusive fluxes. However, further down the pillars and closer to the base of the array, liposome concentrations were below threshold values needed to form cohesive lipid bilayers, instead resulting in intact adsorbed vesicles, mobile lipid patches, and unoccupied surface sites.[34–36] The spatially inhomogeneous fluorescent profiles on the pillars were the result of the system having reached a nonequilibrium steady state (NESS) in the concentration of nonadsorbed, freely diffusing vesicles in solution relatively quickly within the 2 h time window that the pillars were incubated with the vesicle solution. Mechanistic insights gained here will aid in understanding how steady-state diffusive flux in confined environments affect supported lipid bilayer (SLB) formation at the microscale and may lead to practical strategies for improving the uniformity of SLBs formed on micropillars under NESS conditions.

2. Results and Discussion

Large unilamellar vesicles (LUVs) with an average diameter of 130 nm were over an order of magnitude smaller than the 5 µm pillar diameter, which allowed their adsorption to be treated as equivalent to molecular adsorption on a flat surface. The formation of mostly continuous supported lipid bilayer on the pillar top surfaces (roughly 9% defects by area) was confirmed at these locations with liquid-phase tapping-mode atomic force microscopy (AFM) (Supporting Information). The lipid films at the base, however, were discontinuous and comprised of overlapping membrane fragments or patches.

FRAP results (Supporting Information) indicated that most of the surface-adsorbed lipid molecules were laterally mobile both at the pillar tops and at the base substrate between the pillars. However, surface diffusion was considerably slower on the pillar tops than at the base substrate, which, in turn, was slower than on smooth, flat, hydrophilic surfaces such as glass or quartz.[37] The fluorescence recovery on the pillar tops was likely slowed as a result of the lipid membrane being confined within a circle on the pillar top with a radius of 2.5 µm, which was within the range of effective bleach radii determined from the confocal FRAP data. Any lipid molecules outside of this circle would have to migrate over the top edge of the pillar from the sidewall to participate in the fluorescence recovery, which would be energetically costly, resulting in lower effective lipid mobility

Figure 1 is a composite image showing the effects of increasing pillar height on the assembly of supported lipid bilayers and consists of scanning electron microscopy (SEM) images of the pillars (Figure 1a), orthogonal fluorescent views of surfaces along and perpendicular to the pillar sidewalls, and confocal sections of these images from z-stack images were captured with a laser scanning confocal microscope (Figure 1b,c).

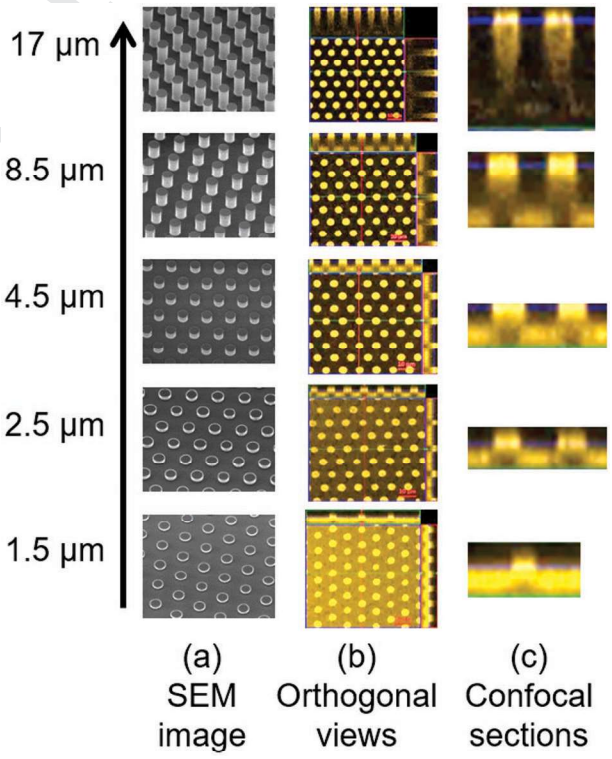

Figure 1. Images of supported lipid bilayers formed from vesicle fusion on micropillars. a) SEM images of the pillar arrays. b) Orthogonal views (radial and axial) and c) confocal sections taken from z-stack images on a laser scanning fluorescence confocal microscope.

UNCORRECTED PROOF

© 2019 WILEY-VCH Verlag GmbH & Co. KGaA, Weinheim

At reduced pillar heights (≤2.5 µm), fluorescence intensity distributions from the pillar sidewalls and between the pillars were similar. However, as pillar height increased, the difference between the profiles increased as well, such that there was an almost complete loss of fluorescence from the base substrate in the case of the tallest (i.e., 8.5, and 17 µm) pillars, while the fluorescent intensities at the pillar tops remained virtually unchanged (Figure 1b,c).

This behavior was further examined using kMC simulations of particles undergoing random walks in an array of pillars. In these simulations, the particles adhered irreversibly upon contact with the pillars, which ranged in height from 1.5 to 17 µm. The distribution of contact points from independent particles is shown in **Figure 2**. The intensities from the images can be regarded as proxies for the experimentally measured fluorescence intensities (compare column 3 in Figure 2 with Figure 1c). Columns 1 and 2 in the figure are images of the simulated vesicle-pillar contact frequencies at the top and bottom of the pillar array. Column 3 shows the simulated cross-sectional views of particle adsorption frequency on the pillar sidewalls. Although there were clear quantitative differences to be discussed in detail below, the qualitative agreement between the simulated images, generated solely by random walk processes and experimental results in Figure 1, highlights the importance that modulation of the diffusive flux by specific boundary conditions had on lipid bilayer assembly. In the model, particles adsorbed preferentially at the pillar tops as a result of their greater accessibility to an effectively semi-infinite space in bulk solution above the pillar array compared to the confined volumes between the pillars and the base substrate.

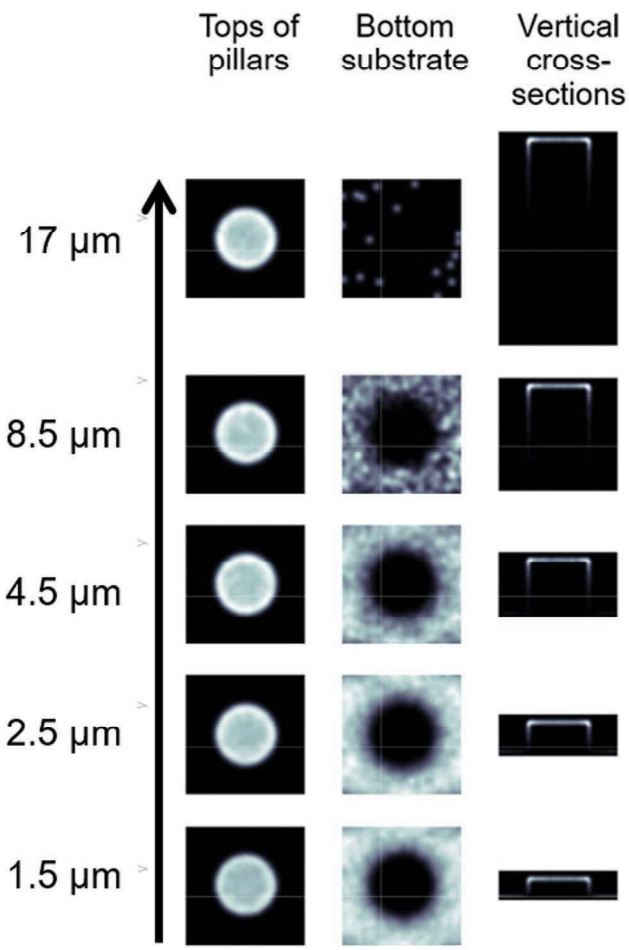

Figure 2. Vesicle adsorption profiles generated by kinetic Monte Carlo simulations of vesicle/pillar contact frequencies.

To understand better how vesicle diffusion was impacted by the confined environment between pillars, we used finite element methods to numerically evaluate the diffusion equation (Fick's second law)

$$\frac{\partial c}{\partial t} = D\nabla^2 c \tag{1}$$

around a single pillar at steady state (**Figure 3**). Here, D is the diffusion coefficient of vesicles in solution ($m^2\ s^{-1}$), c is concentration, and ∇^2 is the Laplace operator. The geometry of the system is shown schematically in Figure 3a,b. The hexagonal unit cell featured a radius b and height h, defined around a central pillar with a smaller radius a. The vertices of the hexagon in Figure 3a extended outward from the middle of the central pillar, which served as the origin, to the point midway to the closest edge of each of its neighbors such that the edge-to-edge separation distance between adjacent pillars was $2 \times (b - a)$. The Laplace operator was expressed in cylindrical coordinates, and azimuthal symmetry was assumed to approximate the effect of multiple nearest-neighbor pillars.

Boundary conditions were specified as follows. The LUV concentration was fixed at the bulk solution-phase vesicle concentration γ_{max}, which was set 10 µm above the pillar tops (h + 10 µm), and the LUV concentration was fixed at zero at all SiO_2–aqueous interfaces. No-flux conditions were adopted at the outer radius of the hexagonal unit cell, that is, at $r = \pm b$ (5 µm). In addition, vesicle adsorption at the interface was assumed to be irreversible, involving vesicle disruption and the formation of supported lipid bilayers (SLBs) on the surface, which depleted the solution of freely diffusing LUVs. Figure 3c displays the steady-state solution for the concentration of vesicles for 17 µm tall pillars separated by 5 µm. The boundaries in the figure at ±5 µm were assumed to be averages of the six neighboring pillars surrounding the central pillar and the free space between them.

The resulting radial diffusive fluxes to the pillar sidewalls were given by

$$J(r,\gamma) = -D\frac{\partial c(r,\gamma)}{\partial r} \tag{2}$$

where J corresponds to the molar diffusive flux (in units mol $m^{-2}\ s^{-1}$), D is the diffusion coefficient for vesicles in solution, and $\frac{\partial c(r,\gamma)}{\partial r}$ is the concentration gradient in cylindrical coordinates. At steady state, the diffusion coefficient did not influence the concentration profiles, but it did affect the fluxes.

The diffusion coefficient, D, was estimated to be $3.8 \times 10^{-12}\ m^2\ s^{-1}$ using the Stokes–Einstein relation

$$D = \frac{kT}{6\pi\eta R} \tag{3}$$

© 2019 WILEY-VCH Verlag GmbH & Co. KGaA, Weinheim

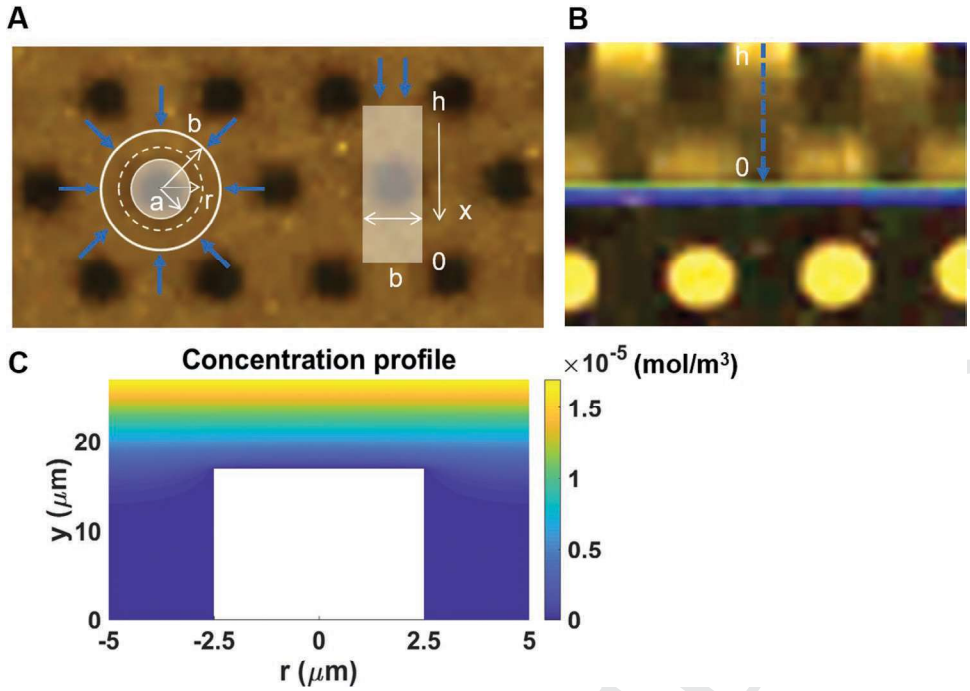

Figure 3. a) Hexagonal unit cell used to parameterize diffusion in the pillar array, overlaid on a top-down image of the array. b) Side-view image of pillars from a confocal orthogonal section (adapted from Figure 1c). c) Finite element simulation of steady-state concentration profile for a 17 µm tall pillar, 5 µm in diameter, separated from neighboring pillars with center-to-center spacings of 10 µm (a = 2.5 µm, b = 5.0 µm).

where k is the Boltzmann constant, T is the temperature (298 K), η is the viscosity of water (0.89 cP), and R is the vesicle radius (65 nm). The assumption that the system had reached a steady state was strengthened by the fact that the estimated 1D diffusion time required for a vesicle to reach the base substrate from bulk solution, given by

$$t = \frac{(y_{\max})^2}{2D} = 80\ \text{s} \tag{4}$$

for the tallest pillars ($y_{\max}$ = 27 µm), was almost two orders of magnitude shorter than the incubation time of 2 h. We further assumed that the adsorption of liposomes on the base and pillar surfaces was irreversible under steady-state conditions, which allowed us to substitute the diffusive flux for the density of adsorbed vesicles on the surface, in line with the use of contact frequencies as surrogates for particle density in the kMC simulations described earlier.

Figure 4 compares steady-state diffusive fluxes with corresponding fluorescence data, both on the pillar sidewalls and at the base of the array. Figure 4a displays the radial diffusive fluxes as functions of vertical position on the pillar sidewalls (y). The solid lines correspond to 5 µm gap distances ($2 \times (b - a)$ = 5 µm) between adjacent pillars in the array, consistent with the experimental geometries, while the dashed lines are predicted results if the gap distances were to increase to $2 \times (b - a)$ = 100 µm. This was done to identify any potential coupling interactions between the pillar pitch and the height, which could affect the diffusive dynamics under confined conditions. Plots of the particle density on the pillar sidewalls as functions of pillar height from the kMC model in Figure 2 were in close agreement with the estimated diffusive fluxes at 5 µm pitch in Figure 4a.

As seen in Figure 4a, the differences in the diffusive flux profiles of pillars with a 5 µm pitch versus those with a 100 µm pitch were negligible for heights <4.5 µm, indicating the sidewall flux profiles for smaller pillars were not sensitive to confinement by neighboring pillars in an array. However, these differences became progressively more pronounced for pillars with height $h \geq 4.5$ µm. For example, the flux profile for the 17 µm tall pillars at 5 µm pillar separation in the panel was very steep near the top of the pillar, and the flux decreased to negligible values over the interval $0 \leq y \leq 12$ µm. While similar steep decreases in flux profiles near the tops were seen for the smaller pillars, they approached zero at the pillar base in a more linear manner. Together, these observations indicate that in-plane confinement affected calculated diffusive fluxes significantly only when the aspect ratios of pillar height to pitch were greater than unity (i.e., for pillar heights $h \geq 5$ µm).

Figure 4b shows the corresponding measured fluorescent profiles versus vertical position along the pillar sidewalls, fit to Gaussian functions. We interpret these fluorescent profiles as being roughly proportional to the steady-state diffusive fluxes in Figure 4a, an assumption supported by the fact that the fluorescent gradients in Figure 1c remained well-defined even though the pillar arrays had been incubating in the vesicle solution for 2 h and then rinsed with buffer before measuring fluorescence. However, these gradients were generally shallower than their calculated diffusive flux counterparts in Figure 4a and were, in fact, more similar to the 100 µm spacing case (dashed curves in Figure 4a) than the 5 µm spacing (solid curves in Figure 4a), even though the actual separation distance in all experiments

UNCORRECTED PROOF

© 2019 WILEY-VCH Verlag GmbH & Co. KGaA, Weinheim

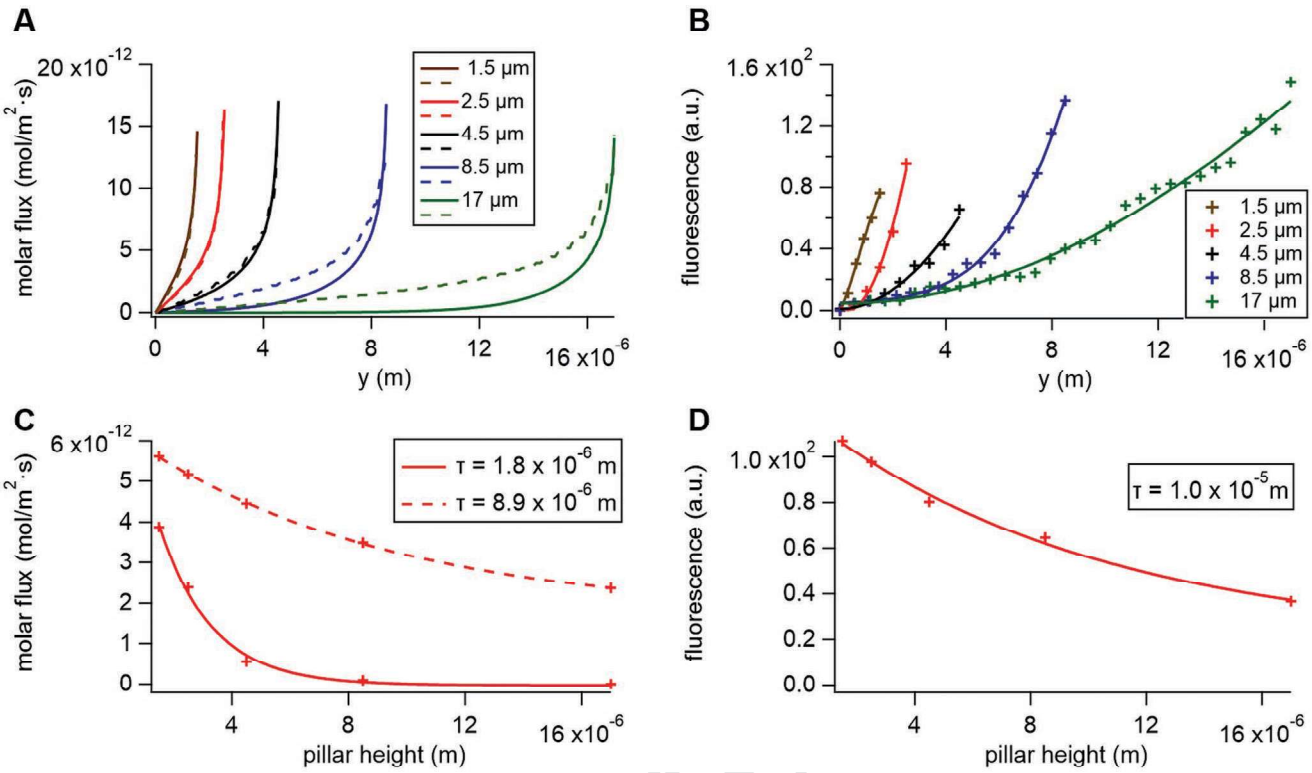

Figure 4. a) Calculated steady-state diffusive fluxes along pillar sidewalls versus vertical position, for 5 µm (solid lines) and 100 µm spacings between pillars (dashed lines). b) Background-subtracted fluorescent gradients along pillar sidewalls versus position (extracted from Figure 1e), fit to Gaussians (solid lines). c) Steady-state diffusive fluxes at the base substrate, located midway between adjacent pillars as functions of pillar height, for 5 µm ($2 \times (b - a) = 5$ µm, solid line) and 100 µm spacings between adjacent pillar sidewalls ($2 \times (b - a) = 100$ µm, dashed line), fit to exponentials. d) Fluorescence intensities at the base of the array, located midway between pillars as functions of pillar height, fit to an exponential. 1/e decay lengths for the plots in (c) and (d) are given in the text boxes.

was 5 µm. We attribute this to the development of confluent supported lipid bilayers around the pillar tops, which resisted additional adsorption and rupture of new vesicles from solution compared to the more isolated mobile lipid bilayer patches and bare spaces available for adsorption further down the pillars.[34–36] This resulted in flatter fluorescent profiles.

Figure 4c,d shows the calculated diffusive fluxes and the average measured fluorescent intensities midway between adjacent pillars and at the base substrate as functions of pillar height, fit to single exponential functions. The solid line in Figure 4c is the best fit to the simulated fluxes for a 5 µm gap between pillar sidewalls, and the dashed line is the best fit for fluxes for a 100 µm gap. The exponential dependencies as functions of pillar height for all three cases, that is, the diffusive fluxes at 5 µm and 100 µm spacings in Figure 4c, and the fluorescence intensities in Figure 4d, suggest that vesicle depletion from solution was a pseudo first-order process in the concentration of freely diffusing vesicles, which would be the case if the effective numbers of sites available for adsorption on the taller pillars were significantly greater than the number of free vesicles in solution. However, because the net depletion of vesicles from solution was less than what was predicted by the model, the reduction in fluorescence intensity as a function of increasing pillar height in Figure 4d was also less than expected. The 1/e decay lengths for the simulated fluxes at the base substrate, located midway between adjacent pillars and separated by 100 µm ($\tau = 9.3$ µm, dashed line in Figure 4c), were significantly greater than those at 5 µm ($\tau = 1.8$ µm, solid line in Figure 4c). The decay length of the fluorescence at the base of the array in Figure 4d was much closer in magnitude to the simulated diffusive flux for the 100 µm pillar separation than that at the actual 5 µm separation used in experiment.

The fluorescent profiles in Figure 4, which included the fluorescent gradients along the pillar sidewalls shown in Figure 4b, and the fluorescent intensities on the base substrate of the array shown in Figure 4d, were less sensitive to pillar height than the steady-state molar diffusive fluxes would indicate (Figure 4a,c). We attribute this to the reduction in the net number of vesicles depleted from solution due to the development and maintenance of confluent supported lipid bilayers in close proximity to the tops of the pillars under steady-state conditions, which prevented further adsorption of LUVs. This resulted in inhomogeneous spatial distributions of lipid bilayer structures on the pillars, varying from continuous supported bilayer at the pillar tops, to fragmented, mobile lipid islands and bare surfaces along the sides of the pillars and closer to the base substrate.

3. Conclusions

In this paper, we described surface adsorption of fluorescently labeled lipid vesicles under confinement in microfabricated

© 2019 WILEY-VCH Verlag GmbH & Co. KGaA, Weinheim

pillar arrays, followed by vesicle fusion to form SLBs on hydrophilic silica micropillars. The fluorescent intensities on the pillars were inhomogeneous and sensitive to pillar height, which we attributed to the system attaining a nonequilibrium steady-state condition during incubation of the pillar arrays in aqueous solutions containing LUVs, before being quenched by rinsing away remaining vesicles in solution. Preferential adsorption of vesicles near the pillar tops progressively depleted the LUVs from solution as the vesicles diffused toward the base substrate from bulk solution outside the pillar array. However, both fluorescent profiles along the pillar sidewalls and the base fluorescent intensities versus pillar height decreased less than expected based on diffusive fluxes, found by numerically solving the diffusion equation and by random-walk diffusion models, neither of which consider membrane formation nor diffusive transport on surfaces. This is consistent with a reduction in the extent of vesicle depletion from solution due to the formation of passivating and mobile SLB membrane films and fragments on the pillar sidewall surfaces, portrayed schematically in **Figure 5**.

Many in-depth kinetic studies have described the steps involved in the formation of supported lipid bilayer membranes on uniform, hydrophilic surfaces, including vesicle adsorption, deformation and rupture, as well as spreading and coalescence of the resulting mobile lipid bilayer fragments into continuous, cohesive films.[34–36] These details were missing in the kMC simulations described earlier, which only considered the kinetics of vesicle diffusion, neglecting reaction-limited vesicle decomposition induced by existing lipid membrane fragments and/or additional adsorbed vesicles.[35]

In this study, the acquisition of time-dependent information on the mechanistic steps of lipid film formation on the surfaces of the pillar array, including the interplay of the dynamics between diffusion, vesicle adsorption, and lipid film formation, was not possible since fluorescence imaging was carried out only after the incubation of pillar arrays with vesicle solution had been halted by rinsing with buffer-only solution. Instead, we captured snapshots of the system "frozen in time" in NESS,[38] which, on the one hand, did not have explicit time dependencies since rates are invariant under steady-state conditions. On the other hand, however, NESS systems often feature the emergence of complex chemical and biological patterns, which generally require nonlinear dynamics and sources of matter and energy.[39] In our case, the sources were the steady-state diffusive fluxes of vesicles from bulk solution, and the sinks were the hydrophilic surfaces of the pillar array and the surrounding oxide background of the base substrate, which resulted in the maintenance of lipid density gradients and surface-bound, diffusive escape routes for mobile lipids and bilayer fragments.

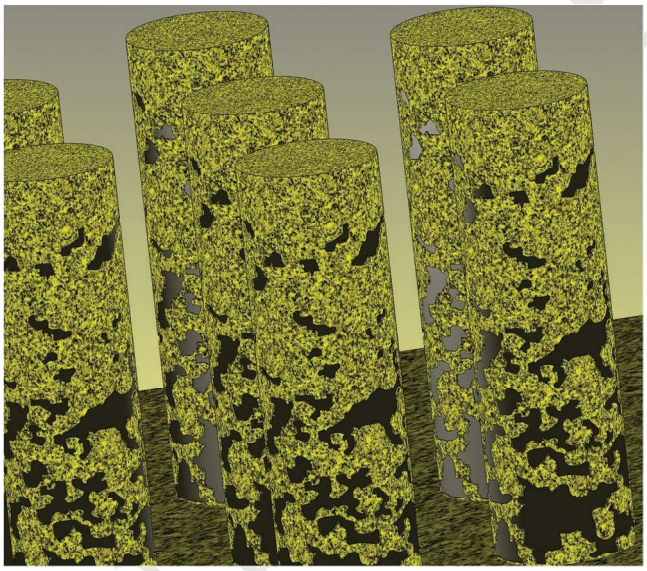

Figure 5. Snapshot of steady-state supported lipid bilayer profiles in an array of 17 µm tall pillars, due to preferential adsorption of lipid vesicles near the pillar tops, coupled with diffusive transport of lipid bilayer and bilayer fragments on pillar surfaces.

The nonlinear dynamics in our system involved interactions between adsorption of vesicles on the pillars, which progressively depleted the vesicles in solution, and passivation of the pillar sidewalls near the pillar tops with supported lipid bilayers formed from the adsorption and rupture of these vesicles, preventing the adsorption of additional vesicles at those sites. Further understanding will require real-time monitoring of emerging inhomogeneous fluorescent intensity profiles in situ on the pillars, systematically varying the incubation times between observations, or both.

Model systems such as these will aid in elucidating how microscale confinement affects emergent properties, including pattern formation in dissipative chemical and biological systems driven in steady states away from equilibrium. Our interpretations of the results described here suggest a strategy for improving the formation of uniform SLBs on the micropillars. AFM and FRAP measurements indicated that the lipid films at the base of the pillar array, while heterogeneous, were nevertheless laterally mobile, highlighting the ability of surface-adsorbed lipids to migrate away from the pillars in the array, even in disordered multilayer structures. This migration, and the resulting steady state, could be disrupted by changing the surface chemical functionalization at the base substrate from hydrophilic to hydrophobic, while keeping the pillars hydrophilic. One example of how this could be accomplished is by using a sacrificial layer strategy for forming hydrophilic silica micropillars on base substrates coated with hydrophobic fluoropolymer.[40]

4. Experimental Section

Substrate Fabrication and Characterization: Micropillars with different heights were fabricated using photolithography followed by reactive ion etching (RIE). The pillars were then conformally coated with ≈25 nm silicon dioxide by atomic layer deposition (ALD). SEM was used to characterize pillar surfaces prior to experimentation. The micropillar diameter was 5 µm and their heights ranged from 1.5 to 17 µm, depending on the reactive ion etching time.

Vesicle Preparations: 1-Palmitoyl-2-oleoyl-*sn*-glycero-3-phosphocholine (POPC) was purchased from Avanti Polar Lipids Inc., and the fluorescent molecule Dil-C12 was obtained from ThermoFisher Scientific. LUVs (1.7×10^{-8}) with an average diameter of 130 nm were prepared by extrusion.[41]

Bilayer Formation via Fusion: Pillar substrates were piranha-cleaned and rinsed thoroughly with deionized (DI) water, rendering them hydrophilic. Substrates were then incubated in vesicle solution for 2 h. Before imaging, excess vesicles were washed away with buffer solution.

© 2019 WILEY-VCH Verlag GmbH & Co. KGaA, Weinheim

AFM Measurements of Lipid Bilayers on Micropillars: AFM topographical imaging was performed on the substrates before and after POPC lipid bilayers were deposited during incubation in LUV solution. AFM imaging was performed in tapping (AC) mode in a droplet of phosphate buffered saline (PBS) solution (10×10^{-3}) using a soft tip. Measurements were performed using an Asylum Research, Cypher system and as-received silicon nitride (Nanosensors, DNP-10) cantilevers.

Fluorescence Microscopy: Fluorescent imaging of supported lipid bilayers on substrates labeled with Dil-C12 was performed in epifluorescence geometry using an inverted confocal laser scanning microscope (Zeiss LSM710) equipped with a 63× oil-immersion objective lens. The substrate was positioned upside down inside a MiTek glass-bottom petri dish and immersed in buffer solution to prevent exposure to air during imaging.

Lipid mobilities (diffusion coefficients) and the fractions of mobile lipids as functions of pillar height were determined by fitting fluorescence recovery curves to a variant of the conventional expression for FRAP that accounts for surface diffusion that occurs during photobleaching, suitable for laser scanning confocal fluorescence microscopy. Experiments were performed at room temperature by photobleaching a circular spot with a 561 nm laser. The recovery curves, together with pre- and post-bleaching profiles, were used to extract in-plane diffusion coefficients on the surfaces in the pillar arrays and the fraction of mobile lipids in the supported bilayers.[42]

kMC Simulations: Particles representing individual vesicles underwent random walks starting from an arbitrary position 10 µm above the top of the cylindrical array of pillars. Pillars were organized in a hexagonal array analogous to those in the actual experiments. The cylinder and substrate surfaces were considered perfectly absorbing, and the contact point of every vesicle was recorded to determine the contact frequency as a function of position.

Numerical Solution of the Diffusion Equation: The Partial Differential Equation (PDE) Toolbox in MATLAB 16a was used to numerically solve the diffusion equation at steady state subject to the boundary conditions described in the text.

Supporting Information

Supporting Information is available from the Wiley Online Library or from the author.

Acknowledgements

Micropillar fabrication and fluorescent imaging and F.L., B.R.S., and C.P.C. were partially supported by the Laboratory Directed Research and Development Program of Oak Ridge National Laboratory, managed by UT-Battelle, LLC, for the U.S. Department of Energy. S.M.A. was supported by a Joint Directed Research and Development award from the UT-ORNL Science Alliance. J.K. was supported through the Scientific User Facilities Division of the Department of Energy (DOE) Office of Science, sponsored by the Basic Energy Sciences (BES) Program, under Contract No. DE-AC05-00OR22725. A portion of this research was conducted at the Center for Nanophase Materials Sciences, which is a DOE Office of Science User Facility. This manuscript was authored by UT-Battelle, LLC, under Contract No. DE-AC0500OR22725 with the U.S. Department of Energy. The U.S. Government retains and the publisher, by accepting the article for publication, acknowledges that the U.S. Government retains a non-exclusive, paid-up, irrevocable, worldwide license to publish or reproduce the published form of this manuscript, or allow others to do so, for the U.S. Government purposes.

Conflict of Interest

The authors declare no conflict of interest.

Keywords

adsorption, diffusion, microfabrication, supported lipid bilayers, vesicles

Received: January 8, 2019
Revised: February 10, 2019
Published online:

[1] T. M. Allen, P. R. Cullis, *Adv. Drug Delivery Rev.* **2013**, *65*, 36.
[2] A. Akbarzadeh, R. Rezaei-Sadabady, S. Davaran, S. W. Joo, N. Zarghami, Y. Hanifehpour, M. Samiei, M. Kouhi, K. Nejati-Koshki, *Nanoscale Res. Lett.* **2013**, *8*, 102.
[3] N. Dogra, H. Izadi, T. K. Vanderlick, *Sci. Rep.* **2016**, *6*, 29369.
[4] S. Bobone, E. Miele, B. Cerroni, D. Roversi, A. Bocedi, E. Nicolai, A. Di Venere, E. Placidi, G. Ricci, N. Rosato, L. Stella, *Langmuir* **2015**, *31*, 7572.
[5] M. Agrawal, Ajazuddin, D. K. Tripathi, S. Saraf, S. Saraf, S. G. Antimisiaris, S. Mourtas, M. Hammarlund-Udenaes, A. Alexander, *J. Controlled Release* **2017**, *260*, 61.
[6] R. Solaro, F. Chiellini, A. Battisti, *Materials* **2010**. *3*, 1928.
[7] A. Mickova, M. Buzgo, O. Benada, M. Rampichova, Z. Fisar, E. Filova, M. Tesarova, D. Lukas, E. Amler, *Biomacromolecules* **2012**, *13*, 952.
[8] G. Cevc, *Adv. Drug Delivery Rev.* **2004**, *56*, 675.
[9] Y. Malam, M. Loizidou, A. M. Seifalian, *Trends Pharmacol. Sci.* **2009**, *30*, 592.
[10] N. Monteiro, A. Martins, R. L. Reis, N. M. Neves, *J. R. Soc., Interface* **2014**, *11*, 20140459.
[11] Y.-H. M. Chan, S. G. Boxer, *Curr. Opin. Chem. Biol.* **2007**, *11*, 581.
[12] E. T. Castellana, P. S. Cremer, *Surf. Sci. Rep.* **2006**, *61*, 429.
[13] R. P. Richter, R. Bérat, A. R. Brisson, *Langmuir* **2006**, *22*, 3497.
[14] A. van Oudenaarden, J. T. Groves, S. G. Boxer, *Biophys. J.* **1999**, *76*, A11.
[15] O. M. Schütte, I. Mey, J. Enderlein, F. Savič, B. Geil, A. Janshoff, C. Steinem, *Proc. Natl. Acad. Sci. USA* **2017**, *114*, E6064.
[16] J. Shi, A. R. Votruba, O. C. Farokhazad, R. Langer, *Nano Lett.* **2010**, *10*, 3223.
[17] C. P. Collier, *Chem. Phys. Lipids* **2015**, *192*, 75.
[18] J. Tamayo, P. M. Kosaka, J. J. Ruz, Á. San Paulo, M. Calleja, *Chem. Soc. Rev.* **2013**, *42*, 1287.
[19] N. K. Reitan, A. Juthajan, T. Lindmo, C. de Lange Davies, *J. Biomed. Opt.* **2008**, *13*, 054040.
[20] R. Raccis, A. Nikoubashman, M. Retsch, U. Jonas, K. Koynov, H.-J. Butt, C. N. Likos, G. Fytas, *ACS Nano* **2011**, *5*, 4607.
[21] K. He, F. B. Khorasani, S. T. Retterer, D. K. Thomas, J. C. Conrad, R. Krishnamoorti, *ACS Nano* **2013**, *7*, 5122.
[22] F. B. Khorasani, D. E. Dunstan, R. Krishnamoorti, J. C. Conrad, *Soft Matter* **2016**, *12*, 8407.
[23] P. S. Burada, P. Hänggi, F. Marchesoni, G. Schmid, P. Talkner, *ChemPhysChem* **2009**, *10*, 45.
[24] J. J. Blum, G. Lawler, M. Reed, I. Shin, *Biophys. J.* **1989**, *56*, 995.
[25] S. Nedelcu, J. U. Sommer, *J. Chem. Phys.* **2013**, *138*, 104905.
[26] J. Siepmann, F. Siepmann, *J. Controlled Release* **2012**, *161*, 351.
[27] N. J. Alvarez, L. M. Walker, S. L. Anna, *Phys. Rev. E* **2010**, *82*, 011604.
[28] J. Kankare, I. A. Vinokurov, *Langmuir* **1999**, *15*, 5591.
[29] E. Vilaseca, I. Pastor, A. Isvoran, S. Madurga, J.-L. Garcés, F. Mas, *Theor. Chem. Acc.* **2011**, *128*, 795.
[30] M. Melli, G. Scoles, M. Lazzarino, *ACS Nano* **2011**, *5*, 7928.
[31] C.-Y. Lee, C.-L. Chang, Y.-N. Wang, L.-M. Fu, *Int. J. Mol. Sci.* **2011**, *12*, 3263.
[32] K. He, S. T. Retterer, B. R. Srijanto, J. C. Conrad, R. Krishnamoorti, *ACS Nano* **2014**, *8*, 4221.

UNCORRECTED PROOF

 © 2019 WILEY-VCH Verlag GmbH & Co. KGaA, Weinheim

[33] J. D. C. Jacob, K. He, S. T. Retterer, R. Krishnamoorti, J. C. Conrad, *Soft Matter* **2015**, *11*, 7515.
[34] Z. Zheng, D. Stroumpoulis, A. Parra, L. Petzold, M. Tirrell, *J. Chem. Phys.* **2006**, *124*, 064904.
[35] V. P. Zhdanov, C. A. Keller, K. Glasmästar, B. Kasemo, *J. Chem. Phys.* **2000**, *112*900.
[36] Y. Min, N. Pesika, J. Zasadzinski, J. Israelachvili, *Langmuir* **2010**, *26*, 8684.
[37] W. Febo-Ayala, D. P. Holland, S. A. Bradley, D. H. Thompson, *Langmuir* **2007**, *23*, 6276.
[38] H. Ge, M. Qian, H. Qian, *Phys. Rep.* **2012**, *510*, 87.
[39] I. Prigogine, I. Lefever, *J. Chem. Phys.* **1968**, *48*, 1695.
[40] H. Zhang, Q. Yan, Q. Xu, C. Xiao, X. Liang, *Sci. Rep.* **2017**, *7*, 3983.
[41] F. A. Heberle, R. S. Petruzielo, J. Pan, P. Drazba, N. Kučerka, R. F. Standaert, G. W. Feigenson, J. Katsaras, *J. Am. Chem. Soc.* **2013**, *135*, 6853.
[42] M. Kang, C. A. Day, A. K. Kenworthy, E. DiBenedetto, *Traffic* **2012**, *13*, 1589.

UNCORRECTED PROOF

 © 2019 WILEY-VCH Verlag GmbH & Co. KGaA, Weinheim